PROCEEDINGS OF THE YEREVAN STATE UNIVERSITY

Chemistry and Biology 2024, **58**(3), p. 173–191

Chemistry

ACID AND HEAT TREATMENT OF ARMENIAN CLINOPTILOLITE

V. G. TSITSISHVILI[1*], N. A. MIRDZVELI[2**], N. M. DOLABERIDZE[2***], M. O. NIJARADZE[2****], Z. S. AMIRIDZE[2*****], B. T. KHUTSISHVILI[2******], L. Sh. TANGAMYAN[3*******], Kh. T. NAZARETYAN[3,4********], H. H. SARGSYAN[3,5*********], A. V. MANUKYAN[3,6**********], L. R. HARUTYUNYAN[3**********]

[1] *Georgian National Academy of Sciences, Georgia*
[2] *P. Melikishvili Institute of Physical and Organic Chemistry, TSU, Georgia*
[3] *Armenian National Agrarian University (ANAU), Armenia*
[4] *Institute of Chemical Physics NAS RA, Armenia*
[5] *H. Buniatian Institute of Biochemistry of NAS of RA, Armenia*
[6] *Mining and Metallurgy Institute, Armenia*

Acid treatment of natural zeolites is often used to “improve” their porous structure and properties, which are also affected by thermal treatment. The influence of hydrochloric acid solutions with concentrations up to 2 *N* and calcination at temperatures up to 800°C on the structure and properties of clinoptilolite-containing tuff from the Armenian Nor-Kohb deposit, selected for the creation of new bactericidal zeolite filter materials for purification and disinfection of water from various sources, was studied by the chemical analysis, powder X-ray diffraction patterns, adsorption of water, benzene and nitrogen. It was found that an acidic environment leads to significant dealumination (Si/Al atomic ratio increases from ≈5 to ≈9.4) and changes in cationic composition without decationization leading to a decrease in the adsorption capacity for water vapor; acidic solutions do not lead to amorphization of the zeolite microporous crystal structure, but gradually dissolve it. Acid treatment also “opens” micropores for large non-polar nitrogen molecules, increases the adsorbing surface area and causes changes in the mesopore system, leading to an increase in their size. Heating leads to the transformation of partially dehydrated zeolite into the metastable phase of heulandite B at 457°C followed by possible formation of zeolite-like mineral wairakite (500°C) and formation of anorthite-like feldspar (600°C); the content of the amorphous phase increases with increasing temperature, but the zeolite crystalline structure is maintained even after annealing at 800°C. The specific porosity of heulandite (0.17 cm^3/g) is maintained up to a temperature of 700°C, the adsorption capacity of micropores for water vapor (>4 *mmol*/*g*) does not change up to a temperature of 500°C, at higher calcination temperatures, the volume of micropores available for nitrogen molecules and the surface area also decrease, and the average diameter of nano-sized pores increases.

https://doi.org/10.46991/PYSUB.2024.58.3.173

***Keywords*:** clinoptilolite, dealumination, decationization, dehydration, amorphization.

* E-mail: v.tsitsishvili@googlemail.com
** E-mail: nato.mirdzveli@gmail.com
*** E-mail: nanuli.dolaberidze@tsu.ge
**** E-mail: manana.nijaradze@tsu.ge
***** E-mail: zurab.amiridze@tsu.ge
****** E-mail: bela.khutsishvili@tsu.ge
******* E-mail: miss.tangamyan@mail.ru
******** E-mail: khachik.nazaretyan@mail.ru
********* E-mail: hakobplus@gmail.com
********** E-mail: alla-man@mail.ru
********** E-mail: l.harutyunyan@anau.am

Introduction. Zeolite-containing tuff from the Nor Kokhb deposit was chosen as one of the main materials for creating new bactericidal zeolite filter materials for purification-decontamination of water from various sources [1]. In general, zeolites consist of an aluminosilicate lattice [$Al_xSi_yO_{2(x+y)}$], constructed from alternating electrically neutral [SiO_4] tetrahedra and negatively charged [AlO_4]$^-$ tetrahedra, forming an open one-, two- or three-dimensional framework with cages and channels. The cavities and channels form a system of micropores, due to which zeolites have molecular sieve and sorption properties, and are very widely used [2]. In addition, zeolites contain labile cations (Na^+, K^+, Ca^{2+}, Mg^{2+}, etc.) that compensate for the negative charge of the framework, and water molecules associated with the framework and cations, which determines the ion-exchange properties of zeolites, allowing them to absorb heavy metal cations [3]. Today, the Database of Zeolite Structures [4] of the International Zeolite Association includes 256 different types of frameworks of natural and synthetic zeolites, but the greatest application, mainly in agriculture and the production of building materials, is found in natural heulandite-clinoptilolites, deposits of which have been found in many countries.

Studies of the zeolite-containing tuff of the Nor Kokhb deposit, constituted of four interbedded layers up to 100 *m* thick and containing about 65–80% clinoptilolite (Cpt) [5], began in the 20th century [6]. Later, the adsorption properties of this natural zeolite [7–9], as well as its chemical and thermal modification [10–13], were studied. The physical properties such as dielectric permittivity, specific conductivity, luminescence and infrared absorption of natural zeolite from the Nor Kokhb deposit were also carried out [14].

The purpose of this paper is to consider changes in the structure and properties of Cpt-containing tuff from the Nor Kokhb deposit under the influence of acid and thermal treatment based on new and previously published data on characterization, dehydration and structural transformations.

Experimental Part.

Materials and Methods. All the reagents were used from commercial sources without further purification with the exception of zeolite. Zeolitic tuff samples were collected at the Nor Kokhb deposit, located in Noyemberyan Region of Armenia. Preparation of zeolite samples included crushing the tuff in a standard crusher, fractionation to a particle size of 1.0–1.4 *mm* (14–16 mesh), washing with distilled water to remove clay impurities, and drying at a temperature of 95–100°C.

Treatment. Acid treatment was carried out by processing 10 *g* of prepared (crushed, sieved, washed and dried) zeolitic tuff with 100 *mL* of 0.5, 1.0, and 2.0 *N* solutions of hydrochloric acid in a shaker (MSH-20A, Daihan Scientific Group,) operating in a linear mode at 75°C. The first step of acid treatment lasted 1 *h*, the second – 2 *h*, and the third – 3 *h*, each step was followed by washing with distilled water at room temperature until no Cl^- ions were detected in the washing water by using $AgNO_3$ solution. The washed and dried samples were weighed to determine the weight loss, the results are given in Tab. 1.

Calcination of the prepared samples, placed in heat-resistant round-bottomed cups, was carried out in a ЭКПС-10 muffle furnace (Smolenskoe SKTB SPU, Russia) in the temperature range of 200–1100°C under static conditions for 1 *h*, then

the cups with calcined zeolite samples were placed in desiccators with calcined $CaCl_2$ until completely cooled.

Table 1

Weight loss (%) from acid treatment steps

Step	Concentration of HCl solution, *N*		
	0.5	1.0	2.0
1st	3.45	3.99	6.04
2nd	3.14	3.42	4.75
3rd	1.14	1.28	1.46

***Characterization*.** Crystallographic analysis was carried out using X'Pert HighScore X-ray diffractometer and software (Malvern Panalytical, UK), continuous scanning was carried out in the 2Θ range from 5°–90° in steps of 0.013° at a scanning speed of 0.09°/*min*. Chemical composition of the original and modified samples was carried out using AAS240FS flame atomic absorption instrument ("Agilent", USA) and standard methods [15–18]. Powder X-ray diffraction (XRD) patterns were obtained on a MiniFlex 600 Rigaku Smart Lab Se diffractometer (Rigaku Corporation, Tokyo, Japan) with a D/teX Ultra 250 1D detector and with Cu-K_α line (λ = 0.154056 *nm*); scanning was carried out in the 2Θ range from 3°–100° in steps of 0.01° at a scanning speed of 2°/*min*. Weight loss, difference thermal analysis (DTA) and difference thermogravimetric (DTG) curves were recorded on a STA 2500 Regulus thermal analyzer (NETZSCH group) at a heating rate of 10°C/*min*.

The adsorption capacity of water vapor and benzene was measured under static conditions at room temperature as follows: the samples were calcined at 260–280°C for an hour, then weighed on an electronic analytical balance FA 2204 *N* (JOAN LAB, China), placed in a desiccator and kept 96 *h* at a constant pressure of water vapor (relative pressure p/p_0 = 0.4 and saturated vapor pressure p/p_0 = 1.0) and benzene (p/p_0 = 1.0), after which samples with absorbate were reweighed. Nitrogen adsorption-desorption isotherms were measured at a temperature of 77 *K* (–196°C) on an ASAP 2020 Plus analyzer (Micromeritics, USA) and a NOVAe 2200 analyzer (Quantochrom, USA).

Results and Discussion.

***Mineralogical and Chemical Composition of Initial Sample*.** According to the analysis of X'Pert powder XRD patterns using Malvern PANalytical database, tuff from the Nor Kokhb deposit contains 58% of calcium Cpt, 25% of sodium Cpt, 7% of kanemite ($HNaSi_2O_5 \cdot 3H_2O$), 5% of quartz (SiO_2), 4% of natrolite (crystal chemical data $|Na_8Cl_2|$ $[Al_6Si_6O_{24}]$-SOD [19]) and 3% of sigma-2 zeolite ($|(C_{10}H_{17}N)_4|$ $[Si_{64}O_{128}]$-SGT [19]). The presence of sigma-2 zeolite, a purely synthetic zeolite-like material with organic template ($C_{10}H_{17}N$ is 1-amino-adamantane), in the sedimentary rock is questionable; most likely, the impurity in question is a type of silicon dioxide.

The results of chemical analysis are expressed by the empirical formula $(Na_{0.29}K_{0.41}Ca_{2.12}Mg_{0.47})$ $[Al_{5.88}Si_{30.1}O_{72}]$, atomic ratio Si/Al = 5.12, rather than for Cpt with Si/Al > 5, which are characterized as high silica clinoptilolites [20].

Chemical Composition of Acid-treated Samples. The results of determining the chemical composition of the acid-treated samples are given in Tab. 2 in the form of averaged empirical formulas of dehydrated zeolites in terms of one aluminum atom to demonstrate changes in the Si/Al atomic ratio, reflecting the degree of dealumination; the sum of the positive charges of sodium, potassium, calcium and magnesium cations per aluminum atom shows the degree of decationization.

Table 2

Chemical composition of original and acid-treated samples

Concentration of HCl solution, *N*	Empirical formula	Compensating charge of cations per Al atom
0	$Na_{0.059}K_{0.153}Ca_{0.333}Mg_{0.0605}$ $[AlSi_{5.12}O_{11.8}]$	1.00 ± 0.06
0.5	$Na_{0.077}K_{0.259}Ca_{0.261}Mg_{0.0708}$ $[AlSi_{6.33}O_{9.82}]$	1.02 ± 0.06
1.0	$Na_{0.0945}K_{0.255}Ca_{0.246}Mg_{0.079}$ $[AlSi_{8.04}O_{7.96}]$	0.94 ± 0.06
2.0	$Na_{0.0947}K_{0.248}Ca_{0.255}Mg_{0.0734}$ $[AlSi_{9.37}O_{6.94}]$	0.96 ± 0.06

As can be seen from the data in Tab. 2, the zeolite undergoes dealumination, and this result is comparable with the data of work [21], in which the treatment of Cpt from the Nor Kokhb deposit was carried out in a solution of hydrochloric acid with a concentration of 1 *mol/L*, at a ratio of liquid and solid phases of 2:1 and a temperature of 95°C for 1.5 *h*, as a result of which the Si/Al atomic ratio increased from 4.3 to 5.46 and to 5.73 under microwave irradiation at a frequency of 2.45 *GHz*.

The total cationic charge in terms of one aluminum atom remains within the measurement error (Tab. 2), although there is a change in the cationic composition shown in Fig. 1, from which it is clear that calcium is washed out along with the leaching of aluminum, while the relative content of relatively large potassium cation increases significantly, and the content of sodium and magnesium increases slightly.

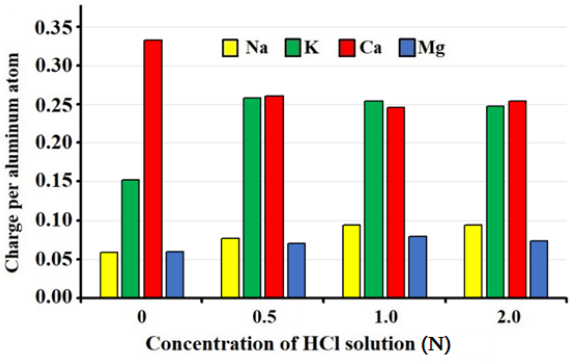


Fig. 1. Changes in cationic charges caused by acid treatment.

A study of the effect of acid treatment on the adsorption properties of high-silica clinoptilolite (Si/Al = 6.22) showed that the removal of monovalent sodium and potassium cations is insignificant over the entire temperature range of 25–100°C and depends little on the acid concentration [22], which corresponds to the results obtained. On the contrary, treatment of aluminum-rich clinoptilolite [23] and heulandite [24] with hydrochloric acid solutions leads to decationization, expressed mainly in the loss of sodium ions Na^+; magnesium Mg^{2+} and calcium Ca^{2+} ions are

washed out to a lesser extent, while relatively large potassium ions K^+ are practically not involved in decationization.

Heat treatment of Nor Kokhb Cpt to certain temperatures only leads to the reversible loss of water molecules. Thermogravimetric analysis [11] showed that the studied Cpt contains approximately one-third more water molecules than follows from the crystal chemical data ($|Ca_4(H_2O)_{24}|$ $[Al_8Si_{28}O_{72}]$-HEU, [15]), which cannot be explained only by the presence of an admixture of kanemite ($HNaSi_2O_5 \cdot 3H_2O$), containing a relatively large number of water molecules. The largest portion of water (70% of the total content) is lost before reaching a temperature of 460°C, the rest of the water molecules leave the crystal lattice continuously during the amorphization process and after its completion at temperatures above 725°C [25].

Structure. Identification of zeolites from powder XRD patterns is based on the 2Θ (°) values of the three most pronounced low-angle reflections [26]. According to simulated patterns, for HEU type zeolites these three reflections are 9.85°, 11.07°, and 22.22° with relative intensities 100%, 64%, and 60%, respectively for heulandite (Si/Al = 2.88), and 9.88°, 11.19°, and 22.49° with relative intensities 100%, 40%, and 49%, respectively for clinoptilolite (Si/Al = 4.84). However, if the first two low-angle peaks are associated with reflections (020) and (200), respectively, then the third peak, observed for Cpt in the range of $22.35° < 2\Theta < 22.81°$, is a superposition of reflections (131), (400), (330), (–421), and (240), which have relative intensities of 49,2%, 18.1%, 37.2%, 21.0%, and 24.4%, respectively. The angular distance between these peaks is very small, and even when scanning speed is less than usual 1°/*min*, the recorded intensity can increase. On the other side, in the XRD patterns of natural heulandite-clinoptilolites with a different Si/Al molar ratio and cation composition, the relative peak intensities may differ from those indicated for simulated patterns. For Georgian heulandite it was noted, that peaks of (020) and (131, 400, etc.) reflections observed at 9.9° and 22.4°, respectively, have high intensities, but the peak from the (200) reflection (11.2°) is rather weak [27].

The assignment of the main intense peaks to the Miller indices for the powder XRD pattern of the original Nor Kokhb Cpt is shown in Fig. 2. As a comparison of the experimental pattern with the simulated one [26] shows, the peak positions are almost identical, but the intensities are significantly different. It is obvious that these differences are associated with differences in cationic composition, since the simulation was carried out for a sample with a similar atomic ratio Si/Al = 4.84, but with a cationic composition of Na ≈ K > Ca > Mg.

As a result of acid treatment, the position of the peaks does not change and their broadening is not observed (XRD patterns of samples treated with hydrochloric acid of different concentrations are given in our work [12]). Thus, the acidic environment does not cause amorphization of Cpt, and the weight loss (Tab. 1) is due to the leaching of Al and the formation of "hydroxyl nests" [28]. However, acid treatment leads to a change in peak intensity (Tab. 3), which is likely due to changes in cationic composition and Al content. In Tab. 3, the *hkl* Miller indices and *d*-spacings are given in accordance with the simulated spectrum [26], the experimentally determined angles 2Θ are given for CuK_α radiation (λ = 1.5418 Å), and the intensity of the peak of the (020) reflection is taken as 100% to represent the relative intensities ($I/I_0 \cdot 100\%$).

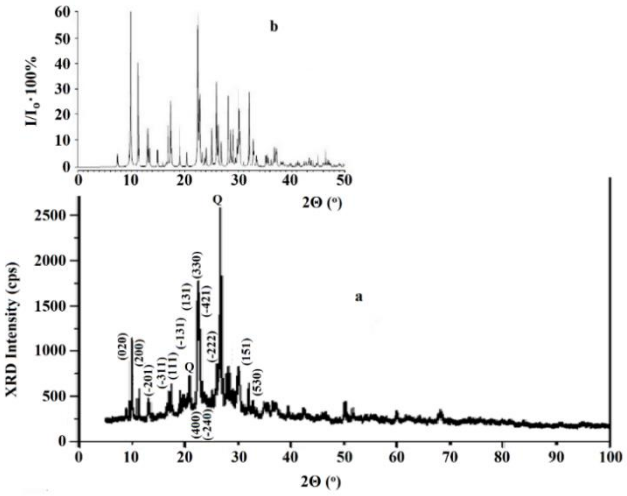


Fig. 2. Powder XRD patterns of original Nor Kokhb sample (a is a numbers in parentheses are Miller indices, *Q* is a peak of quartz) compared with simulated pattern from [25] (b).

Table 3

X-ray data of intense peaks (I/I_o>10%) of natural and acid-treated clinoptilolites

hkl	*d*, Å	Natural		After 0.5 *N*		After 1.0 *N*		After 2.0 *N*	
		2*Θ*	I/I_0, %	2*Θ*	I/I_0, %	2*Θ*	I/I_0, %	2*Θ*	I/I_0, %
020	8.955	9.90	100	9.84	100	9.89	100	9.89	100
200	7.91	11.22	32.9	11.17	30.2	11.20	29.6	11.21	30.8
–201	6.78	13.09	21.9	13.05	30.7	13.10	16.2	13.08	38.9
–311 111	5.243 5.110	17.38	46.2	17.32	28.8	17.39	34.7	17.37	37.2
–131	4.648	19.07	31.3	19.00	21.8	19.06	22.8	19.07	27.3
131 400 330 –421 240	3.976 3.955 3.952 3.916 3.897	22.39 22.75	245 104.3	22.37 22.72	262 54.4	22.42 22.77	248 51.4	22.41 22.77	280 62.6
–222	3.421	26.03	38.3	25.98	31.9	26.05	47.2	26.03	37.6
151	2.973	30.06	115.3	29.97	123	30.03	111	30.09	130
530	2.796	31.99	44.2	31.97	36.1	32.00	34.5	31.96	38.6

As can be seen from Tab. 3, the intensity of peak (200) remains approximately constant (31.25 ± 1.65%), the intensity of peaks (151) and (530) changes slightly (120 ± 10% and 39.4 ± 4.8%, respectively) and non-monotonically, the intensity of the remaining peaks also changes non-monotonically; the intensity of the peaks in the range $22.35° < 2\Theta < 22.5°$ remains high and increases, the intensity of the peaks in the range $22.5° < 2\Theta < 22.8°$ decreases. Apparently, the observed effects are associated with the redistribution of cations.

In addition, after treatment with a HCl solution with a concentration of 0.5 *N*, the value of the angle 2*Θ* of the (020) reflection, sensitive to compression and expansion along the *b* axis (Fig. 2), decreases, indicating an increase in the d_{020}-spacing by ≈0.06 Å. However, treatment with more concentrated solutions results in less

expansion. Changes in the position of the peak of the (200) reflection indicate a similar expansion along the *a* axis, but on a smaller scale, up to ≈0.05 Å (see Fig. 3).

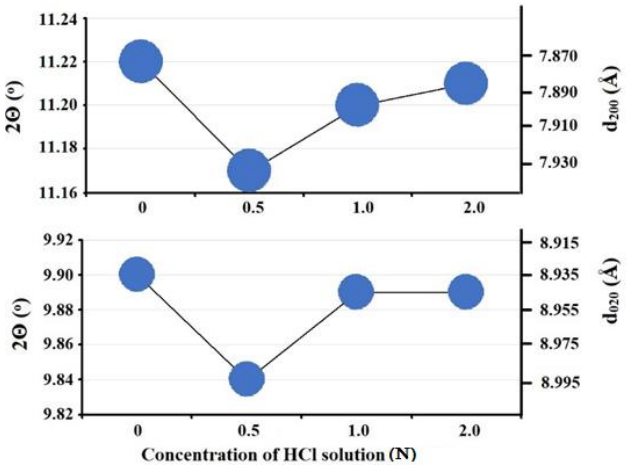


Fig. 3. Change in the position of observed peaks of the (020) and (200) reflections after acid treatment (the size of the circles corresponds to the accuracy of measuring angles 2Θ).

Thermal Stability. It is believed that typical heulandites and clinoptilolites are clearly distinguished by DTA curves [20] and in generally in terms of their thermal stability: according to Mumpton, no transitions or reactions occur in Cpt up to approximately 750°C, while heulandite is much less resistant to thermal treatment [29]. Under the influence of heat, HEU-type zeolites transform into a metastable phase called heulandite B, and in the DTA curve of high-silica heulandite this transition is expressed in a sharp endothermic peak at ≈340°C, but in the DTA curves of clinoptilolite this peak is absent since the transition to the metastable phase occurs at higher temperatures [20].

According to previously obtained thermogravimetric analysis data [11], on the DTG and DTA curves, endo-effects are observed at ≈105°C and ≈210°C, reflecting two stages of the dehydration process, as well as high-temperature endothermic peaks at ≈600°C, ≈690°C (DTG) and 725°C (DTA), corresponding to the destruction of the crystal structure; a weak endo-effect at a temperature of 457°C, probably associated with the formation of a new phase, is recorded only on the DTG curve. Thus, Nor Kokhb clinoptilolite is structurally stable at least up to a temperature of 600°C, which is consistent with the results of a recent study [25].

In powder XRD patterns of calcined samples, as well as for acid-treated samples, a change in the intensity of the peaks is observed, and also, with increasing calcination temperature, the zeolite peaks broaden, a wide "hump" of the amorphous phase and additional peaks appear.

Additional peaks in the range $27.5° < 2\Theta < 28.5°$ are clearly visible in the X-ray diffraction pattern of the sample calcined at 600°C (Fig. 4).

The intense XRD peaks at $2\Theta \approx 28°$ are typical of plagioclase feldspar mineral series, the endmember of which are sodium albite ($NaAlSi_3O_8$), calcium anorthite ($CaA_2lSi_2O_8$) and potassium orthoclase ($KAlSi_3O_8$). The formation of albite at higher temperatures (700–800°C) has been established in sodium-rich heulandite from the Dzegvi-Tedzami deposit, Georgia, and in a calcium-rich mixture of heulandite and chabazite from the Chankanay deposit, Kazakhstan.

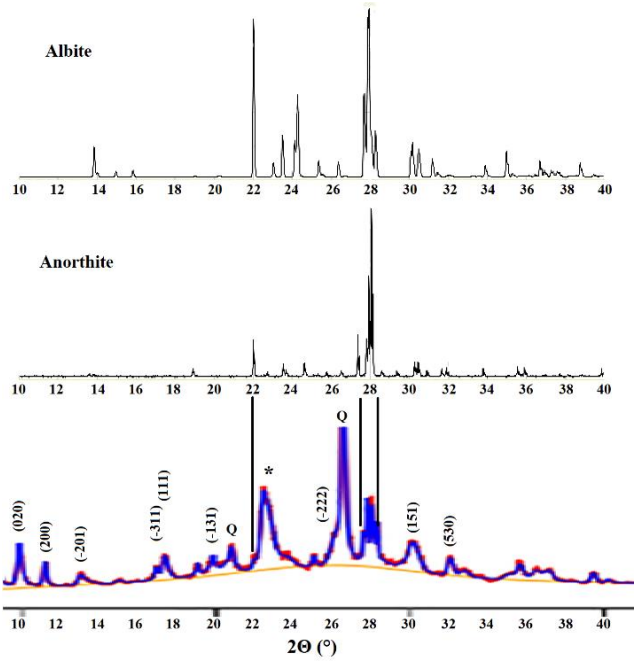


Fig. 4. Powder XRD pattern of Nor Kokhb sample calcined at 600 °C (numbers in parentheses are Miller indices, * – peaks of (131), (400), (330), (–421) and (240) reflections, Q – peaks of quartz) compared with patterns of anorthite and albite from the RRUFF database.

The powder XRD pattern of albite (https://rruff.info/Albite/R100169) is also characterized by a strong peak at $2\Theta = 22.0°$, which is not visible in the XRD patterns of Nor Kokhb clinoptilolite calcined at high temperatures. In the XRD pattern of anorthite (https://rruff.info/Anorthite/R040059) the peak at $2\Theta = 22.0°$ is quite weak, and a comparison of the XRD patterns suggests that in the calcium-rich Nor Kokhb clinoptilolite at high temperatures anorthite-type feldspar is formed.

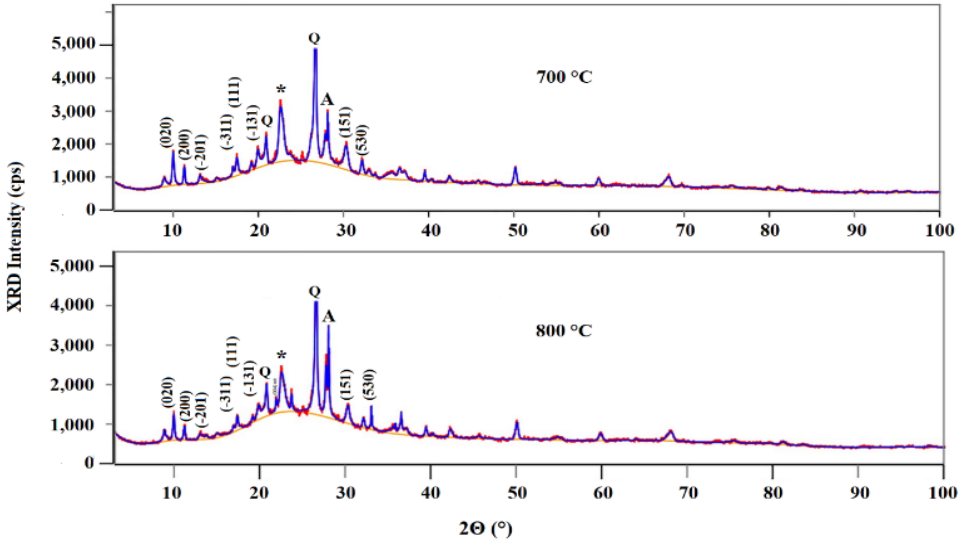


Fig. 5. Powder XRD patterns of Nor Kokhb samples calcined at 700°C and 800°C (numbers in parentheses are Miller indices; * – peaks of (131), (400), (330), (–421) and (240) reflections, *Q* – peaks of quartz, *A* – peak of anorthite).

As the calcination temperature increases, the intensity of the feldspar peaks increases, and the "hump" of the amorphous phase also increases due to a general decrease in the intensity of the peaks, however, the "zeolite" peaks of clinoptilolite remain even after annealing the sample at 800°C (Fig. 5). X-ray data of intense peaks of calcined clinoptilolites are given in Tab. 4 in the same format as in Tab. 3 for the acid-treated samples.

Table 4

X-ray data of intense peaks (I/I_0>10%) of calcined clinoptilolites

hkl	*d*, Å	200°C		300°C		400°C		500°C		600°C		700°C		800°C	
		2Θ	I/I_0	2Θ	I/I_0	2Θ	I/I_0	2Θ	I/I_0	2Θ	I/I_0	2Θ	I/I_0	2Θ	I/I_0
020	8.955	9.89	100	9.89	100	9.94	100	9.94	100	9.82	100	9.97	100	9.96	100
200	7.91	11.19	35.1	11.21	34.4	11.26	30.2	11.27	29.1	11.14	38.1	11.29	36.0	11.22	44.0
–201	6.78	13.10	32.7	13.08	22.4	13.12	18.3	13.13	25.9	12.97	20.4	13.13	43.1	13.03	60.5
–311 111	5.243 5.110	17.37	71.9	17.34	53.8	17.41	31.1	17.41	58.8	17.30	56.5	17.32	61.6	17.35	56.7
–131	4.648	19.06	35.3	19.00	24.0	19.13	28.9	19.14	23.1	19.04	15.6	19.16	23.0	19.18	21.6
131 400 330 –421 240	3.976 3.955 3.952 3.916 3.897	22.43 22.77	273 72.8	22.44 22.71	133 216	22.49 22.78	121 205	22.48 22.74	84.0 183	22.34 22.74	69.1 –	22.56 22.74	340 –	22.51 22.74	398 –
–222	3.421	26.13	132	26.04	51.4	26.11	66.4	26.09	36.2	26.15	129	26.39	–	26.39	–
151	2.973	30.09	158	30.08	124	30.14	113	30.05	82.7	30.07	130	30.23	148	30.30	109
530	2.796	32.02	56.6	31.98	46.8	32.05	39.6	32.09	39.1	31.95	35.7	32.11	48.9	32.09	40.3

With increasing calcination temperature, the intensity of the peaks changes non-monotonically. Thus, the intensity of peaks (–311) and (111) at $2\Theta \approx 13°$ reaches a maximum after calcination at 200°C, then a minimum after heating to 400°C, and then increases and remains high even after annealing at 800°C. The intensity of the peaks in the range $22.35° < 2\Theta < 22.5°$ first increases slightly, and after treatment at 300°C it begins to decrease and reaches a minimum after annealing at 600°C, and then sharply increases, which may indicate the formation of feldspar structure. As for the peaks in the range $22.5^o < 2\Theta < 22.8^o$, their intensity changes insignificantly, after heating at 300°C begins to decrease monotonically and disappears after annealing at 600°C and higher temperatures, as well as the peak of reflection (222) that disappears at 700°C and higher temperature.

The changes in the position of the peaks (020) and (200) are non-monotonic (Fig. 6) and demonstrate a jump in the temperature range of 500–700°C, indicating expansion and subsequent compression along the *a* and *b* axes by approximately 0.12 Å.

It is believed that in clinoptilolites the transition to the metastable heulandite B phase occurs at higher temperatures than in heulandites – at 600–700°C and 340°C, respectively; in Cpt the transition leads to compression along the *b* axis and a decrease in d_{020}-spacing by 0.7–0.8 Å [20].

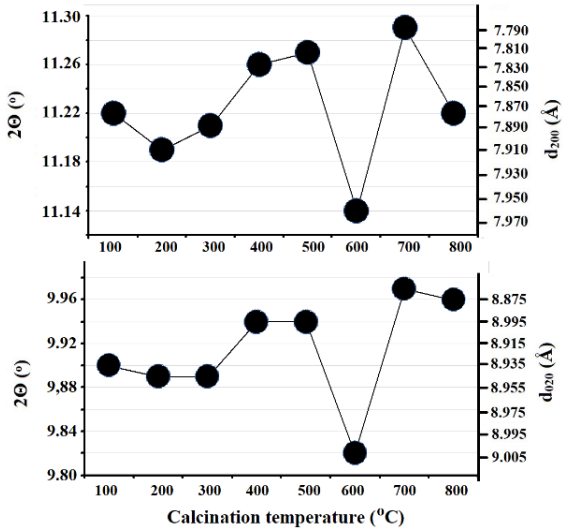


Fig. 6. Change in the position of observed peaks of the (020) and (200) reflections after thermal treatment (the size of the circles corresponds to the accuracy of measuring angles 2Θ).

The effect observed for the studied Nor Kokhb Cpt is much weaker, but the DTG curve shows endothermic effect at a temperature of 457°C that may be associated with the formation of heulandite B phase. In high-silica heulandite, the metastable phase formed at 340°C at temperatures above 500°C forms quartz and the 9.GB.05 group mineral wairakite containing "zeolitic" water, which is shown for a sample of natural heulandite that does not initially contain quartz [30]. Nor Kokhb Cpt contains 7% of quartz and the X-ray diffraction pattern clearly distinguishes a weak peak at $2\Theta = 20.8°$ and a strong peak at $2\Theta = 26.6°$, their relative intensity does not change as a result of calcination of samples at temperatures up to 500°C, but at higher temperatures increases sharply. Although peak broadening is observed in the same temperature range, it can be assumed that the quartz content in annealed samples increases, which may be accompanied by the formation of wairakite, and at higher annealing temperatures, anorthite. Be that as it may, the visible expansion along the *a* and *b* axes after annealing at 600°C indicates a change in the structure of clinoptilolite that does not lead to the collapse of the zeolite crystal structure, as follows from the XRD patterns of samples calcined at high temperatures.

Adsorption of Water and Benzene. The water molecule has a small kinetic diameter of 0.266 *nm* and freely passes through the clinoptilolite entrance windows with a diameter of over 0.3 *nm*. Adsorption of water vapor at a relative pressure $p/p_0 = 0.4$ corresponds to almost complete filling of zeolite micropores, therefore, this value is a measure of the volume of micropores available for small polar molecules [31], while adsorption at a pressure of saturated water vapor ($p/p_0 \approx 1$) is used as a measure of total pore volume. Benzene is a nonpolar and large (kinetic diameter 0.585 *nm*) molecule that does not penetrate clinoptilolite cages and channels, and can only be adsorbed on the outer surface of the zeolite, so the adsorption capacity of benzene is a relative measure of surface area and its hydrophobicity. The adsorption capacity for water vapor (relative pressure p/p_0 of 0.4 and 1.0) and benzene (relative pressure of 1.0) of the acid and heat treated Armenian clinoptilolite is shown in Fig. 7.

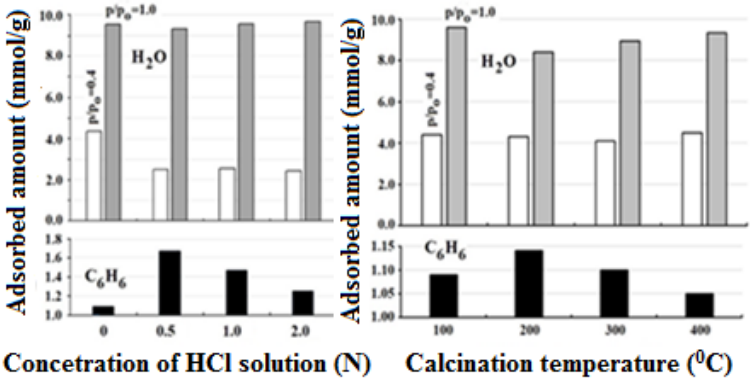


Fig. 7. Water vapor (H_2O) and benzene (C_6H_6) adsorption capacity of acid-treated (left) and calcined (right) samples of Nor Kokhb clinoptilolite.

As a result of acid treatment, water adsorption in the micropores of Armenian clinoptilolite decreases from 4.4 to 2.5 *mmol*/*g*, and this cannot be explained by a decrease in the content of framework aluminum, since the adsorption of water in acid-treated samples is 2.50 ± 0.06 *mmol*/*g* and is practically independent of the acid concentration. This effect can be explained by the redistribution of the cationic composition shown in Fig. 1, as a result of which the role of the relatively large potassium K^+ cation increases and it occupies a larger part of the adsorption space.The water absorption index at saturated vapor pressure $p/p_0 = 1.0$ retains its value 9.5 ± 0.15 *mmol*/*g* even after acid treatment, this corresponds to the data obtained using complete isotherms of water vapor adsorption [32] on high-silica Cpt with a different cationic composition (Si/Al = 6.22, (Na+K) > Ca). Thus, the specific porosity of Nor Kokhb clinoptilolite can be estimated as ≈0.17 ± 0.003 cm^3/g.

The values of adsorption of water vapor in micropores and benzene molecules on the surface of the Nor Kokhb Cpt when the calcination temperature of the samples increases to 400°C (see Fig. 3 right) change within the measurement error; the adsorption of water at saturated vapor pressure also changes insignificantly. At higher temperatures of calcination of samples, adsorption in micropores sharply decreases and becomes irreproducible, while the total adsorption capacity for water vapor decreases by no more than 12%, which indicates an insignificant effect of heat treatment on the specific volume of mesopores.

Adsorption of Nitrogen. A nitrogen molecule with a kinetic diameter of 0.364 *nm* can pass only into one entrance window of clinoptilolite micropores (8-membered ring with sizes of 0.46×0.36 *nm*), whereas 10-membered ring (0.75×0.31 *nm*) and the second 8-membered ring (0.47×0.28 *nm*) cannot accommodate N_2 molecule.

According to the Brunauer–Deming–Deming–Teller classification adopted by IUPAC [33], low-temperature isotherms of nitrogen adsorption-desorption on initial (Fig. 8), acid-treated and calcined samples of Nor Kokhb Cpt belong to type IV, which describes the complete filling of pores: at low relative pressures ($p/p_0 < 0.4$) reflecting the filling of micropores, and showing a hysteresis loop that is a combination of the H_3 loop in the region medium pressures ($0.4 < p/p_0 < 0.9$), characteristic of filling and emptying of slit-shaped pores, and loop H_1 in the

region of high relative pressures ($0.9 < p/p_0 < 1.0$, filling and emptying of cylindrical channels) [34].

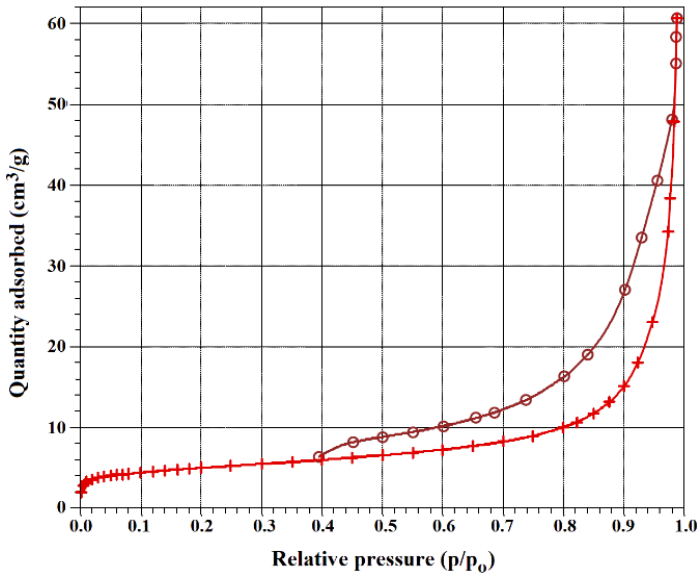


Fig. 8. N_2 adsorption-desorption isotherms on initial sample of Nor Kokhb clinoptilolite.

Isotherms make it possible to calculate the total volume of pores V_p filled by nitrogen molecules from the maximum amount of adsorbed nitrogen gas $Q_{1.0}$, measured at saturated pressure ($Q_{1.0}$ = 60.6 cm^3/g for initial sample) (Fig. 6), and also from the amount of nitrogen $Q_{0.4}$ adsorbed at a relative pressure p/p_0 = 0.4 ($Q_{0.4}$ = 5.975 cm^3/g for initial sample) to estimate micropore volume V_m available for nitrogen molecules.

Experimental data in the range of relative pressures up to $p/p_0 \approx 0.2$ are well described by the Brunauer–Emmett–Teller (BET [35]) equation

$$(\{W[(p/p_0) - 1]\}^{-1} = (W_m C)^{-1} + \{[(C - 1)/W_m C)]\ (p/p_0)\},$$

where W is the adsorption at pressure p; W_m is the monolayer volume on the adsorbent surface; C is the ratio of the adsorption equilibrium constant in the first layer and the condensation constant. The BET isotherm plot and surface area plot are shown in Fig. 9.

For an untreated sample, constant C is 292 ± 18, for modified samples it decreases slightly, but still remains $C \gg 1$ and the BET equation is simplified to

$$\{W[(p/p_0) - 1]\}^{-1} = [(p/p_0)/W_m].$$

The monolayer volume W_m can be determined with high accuracy (±0.1 – 0.25%) from the slope of the BET surface area plot, and the surface area S_{BET} can be calculated from the formula

$$S_{BET} = W_m N_A A_x / M,$$

where N_A is the Avogadro constant ($6.023 \cdot 10^{23}$ mol^{-1}); A_x is the effective cross-sectional area of N_2 molecule (0.162 nm^2); V is the molar volume (22.414 L/mol).

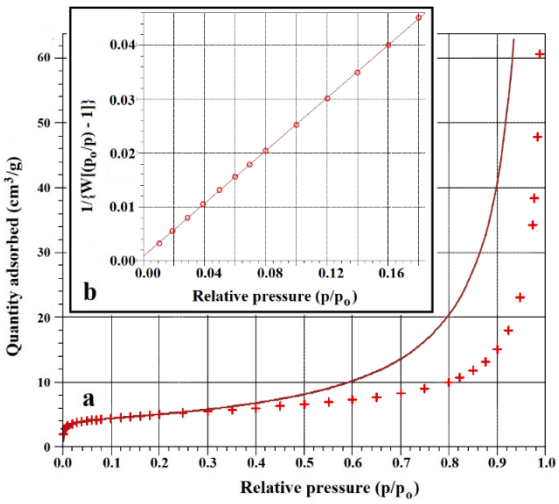


Fig. 9. BET isotherm plot (a, solid line – calculation according to the BET equation, crosses – measured values of adsorption) and BET surface area plot (b).

Estimation of the mesopore size and calculation of the pore size distribution was carried out by the Barrett–Joyner–Halenda (BJH) method [36]. The average pore diameter was calculated from desorption isotherms as $D_{BJH} = 2(r_k + t)$, where the critical radius r_k (Å) = $4.15/[\log(p_0/p)]$ for nitrogen desorption at 77 *K*, and the statistical thickness t (Å) = $3.54[5/\log(p_0/p)]^{0.333}$, according to the Halsey equation [37] and Faass correction [38]. Porosity parameters including total pore volume V_p and micropore volume V_m filled with nitrogen molecules, surface area S_{BET} and average pore diameter D_{BJH} calculated on the basis of experimental adsorption-desorption isotherms on initial, acid-treated and calcined samples are given in Tab. 5, the pore size distribution, curves are shown in Fig. 10.

Table 5

Porosity parameters of initial, acid treated and calcined samples of Nor Kokhb clinoptilolite

Parameter	Initial	Concentration of HCl, *N*			Calcination temperature, °C				
		0.5	1.0	2.0	300	400	500	600	700
V_p, cm^3/g	0.0938	0.102	0.116	0.132	0.0939	0.107	0.0925	0.0940	0.0952
V_m, mm^3/g	9.24	25.5	33.5	42.5	8.61	8.84	4.82	3.34	2.35
S_{BET}, m^2/g	17.7	21.4	36.2	37.7	16.9	16.7	14.7	10.3	8.5
D_{BJH}, *nm*	15.3	21.7	26.7	35.4	16.1	16.7	9.9	12.0	10.6

In contrast to the results for water vapor adsorption, the total pore volume V_p and micropore volume V_m filled with nitrogen molecules increase as a result of acid treatment and with increasing acid concentration. As for the micropores, this is due to the fact that the volume of micropores accessible to nitrogen molecules in the untreated Nor Kokhb clinoptilolite sample is ≈10% of the total pore volume, which is less than the relative volume of micropores accessible to water molecules (≈45%). Taking into account the specific porosity of Nor Kokhb Cpt estimated from the adsorption of water vapor (0.17 *g*/*g*), for the initial sample, nitrogen molecules fill only 55% of the volume of all pores; acid treatment leads to an increase in the degree of filling of all pores with non-polar nitrogen molecules to 78%. Such an “opening”

of micropores and mesopores correlates with an increase in the surface area S_{BET}, and an increase in the diameter of nano-sized pores D_{BJH} reflects changes in the mesopore system.

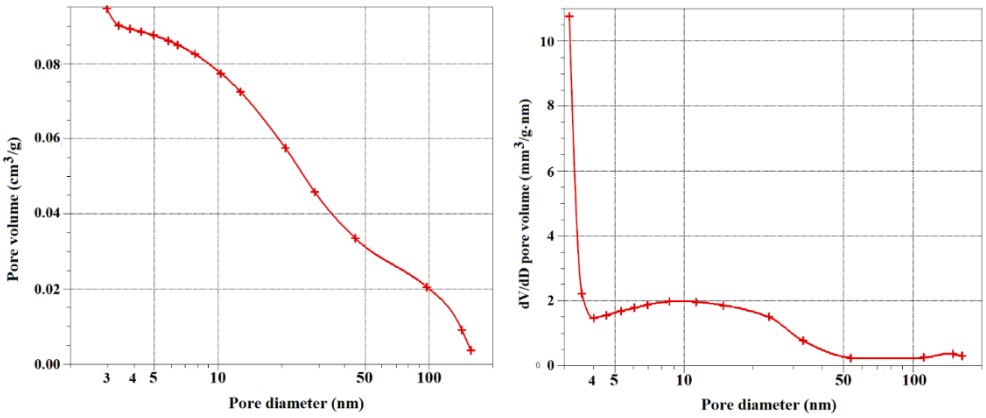


Fig. 10. Pore size distribution volume V vs. pore diameter D (left) and differential dV/dD vs. pore diameter (right) curves calculated by BJH model for initial Nor Kokhb clinoptilolite.

According to the dV/dD differential curve, Nor Kokhb Cpt is characterized by a wide distribution of mesopore sizes, which has two maxima, one corresponding to nano-sized pores with a diameter of less than 4 *nm*, and the second to pores with a diameter of up to 50 *nm* (see Fig. 10, right). As a result of acid treatment, the first maximum increases slightly, indicating an increase in the number of nano-sized pores, and the second maximum "blurs", indicating the appearance of larger mesopores.

To measure nitrogen adsorption-desorption isotherms, the samples are subjected to degassing at a relatively high temperature; the process can take several hours, so adequate data can only be obtained for samples that were calcined at temperatures of 300°C and higher. As evidenced by the results obtained, heat treatment has little effect on the total pore volume; V_p after calcination at 400°C has the greatest value, and with increasing annealing temperature it decreases slightly. The volume of micropores and surface area S_{BET} begin to decrease after calcination at 500°C, and it is obvious that this is due to the amorphization process. The average pore diameter D_{BJH} has a minimum value after calcination at 500°C, but at higher annealing temperatures it increases slightly, although the form of the pore size distribution curves $V(D)$ and even $dV(D)/dD$ is practically not affected by heat treatment.

Conclusion. Taking into account the results of the study, the effect of acid and heat treatment on the structure and properties of clinoptilolite-containing tuff of the Nor Kokhb, the following conclusions can be drawn.

- Treatment of tuff with hydrochloric acid solutions leads to significant dealumination and changes in cationic composition without decationization. A change in the cationic composition of samples treated with acid leads to a decrease in the adsorption capacity for water vapor. Solutions of hydrochloric acid with a concentration of up to 2.0 *N* do not lead to amorphization of the microporous

crystalline structure of zeolite, but are capable of gradually dissolving it. Acid treatment "opens" micropores for large non-polar nitrogen molecules, increases the adsorbing surface area and causes changes in the mesopore system, leading to an increase in their size.

- Under the influence of heat, clinoptilolite at 457℃ transforms into the metastable phase of heulandite B, at 500℃ the formation of quartz and mineral wairakite is possible, at 600℃ anorthite-like feldspar and an amorphous phase are formed, but the zeolite crystalline structure is not destroyed, it is preserved even after annealing at 800℃. Heat treatment reduces the specific porosity of clinoptilolite ($0.17\ cm^3/g$) only at fairly high temperatures ($\geq$ 700℃), and a relatively high adsorption capacity for water vapor ($> 4\ mmol/g$) is maintained after heat treatment at temperatures below 500℃; at higher annealing temperatures, the volume of micropores accessible to nitrogen molecules and the surface area S_{BET} also decrease, while the average diameter of nano-sized pores D_{BJH} increases.
- The results obtained show the possibilities to change structure and properties of Nor Kokhb clinoptilolite-containing tuff and obtain new molecular sieves, adsorbents and ion exchangers.

The authors express their gratitude to the International Science and Technology Center (ISTC) for the support of this work under the project GE-2506 "Scientific substantiation of the possibility of creating new bactericidal zeolite filter materials for purification-decontamination of water from various sources".

Received 10.10.2024
Reviewed 20.11.2024
Accepted 04.12.2024

REFERENCES

1. Tsitsishvili V., Panayotova M., et al. Characterization of Georgian, Kazakh and Armenian Natural Heulandite-Clinoptilolites. *Bull. Georg. Natl Acad. Sci.* **16** (2022), 39–46.
2. Vasconcelos A.A., Len T., et al. Zeolites: A Theoretical and Practical Approach with Uses in (Bio)Chemical Processes. *App. Sci.* **13**(3) (2023). Article Number 1897. https://doi.org/10.3390/app13031897
3. de Magalhães L.F., da Silva G.R., Peres A.E.C. Zeolite Application in Wastewater Treatment. *Adsorpt. Sci. Technol*. **2022** (2022). https://doi.org/10.1155/2022/4544
4. Database of Zeolite Structures https://america.iza-structure.org/IZA-SC/ftc_table.php
5. Sedimentary Zeolite Deposits in Armenia http://www.iza-online.org/natural/Catalog/Armenia.pdf
6. Petrosov I.Kh., Sadoyan A.A. New Zeolite Deposits Spread in Armenia. *Proc. of NAS RA. Earth Sciences* **2** (1998), 39–43 (in Russian).
7. Gevorkyan R.G., Sargsyan H.H., et al. Study of Absorption Properties of Modified Zeolites. *Geochemistry* **62** (2002), 237–242. https://doi.org/10.1078/0009-2819-00014
8. Keheyan Y., Khachatryan S., et al. Sorption Behavior of Tritiated Water on Armenian Natural Zeolites. *J. Radioanal. Nucl. Chem*. **264** (2005), 671–677. https://doi.org/10.1007/s10967-005-0769-7
9. Tsitsishvili V., Machaladze T., et al. Dehydration and Structural Transformations during Thermal Treatment of Georgian, Kazakhstani and Armenian Natural Heulandite-Clinoptilolites. *Scientific collection «InterConf+»* **136** (2022), 356–364.

10. Christidis G.E., Moraetis D., et al. Chemical and Thermal Modification of Natural HEU-Type Zeolitic Materials from Armenia, Georgia and Greece. *Applied Clay Science* **24** (2003), 79–91. https://doi.org/10.1016/S0169-1317(03)00150-9
11. Tsitsishvili V., Dolaberidze N., et al. Acid Treatment of Georgian, Kazakhstani and Armenian Natural Heulandite-Clinoptilolites. *Scientific collection* «*InterConf*+» **138** (2022), 363–370.
12. Tsitsishvili V., Dolaberidze N., et al. Acid Treatment of Georgian, Kazakhstani and Armenian Natural Heulandite-Clinoptilolites. II: Adsorption and Porous Structure. *Scientific collection* «*InterConf*+» (2023). https://doi.org/10.51582/interconf.19-20.03.2023
13. Tsitsishvili V., Dolaberidze N., et al. Thermal Treatment of Georgian, Kazakhstani and Armenian Natural Heulandite-Clinoptilolites. *Scientific collection* «*InterConf*+» **31** (2023). https://doi.org/10.51582/interconf.19-20.01.2023
14. Yeritsyan H.N, Nickoghosyan S.K., et al. Comparative Analyses of Physical Properties of Natural Zeolites from Armenia and USA. *Studies in Surface Science and Catalysis* (eds. A. Gédéon, P. Massiani, F. Babonneau). *Elsevier* **174** A (2008), 529–532. https://doi.org/10.1016/S0167-2991(08)80256-X
15. Copper and Complex Ores, and Products of Their Processing. Method for Measurement of Iron Weight Fraction. *Euro-Asian Interstate Council for Standardization. Metrology and Certification* (2014). https://internet-law.ru/gosts/gost/60060/
16. Copper and Complex Ores, and Products of Their Processing. Methods of Measurement of Silicon Dioxide Weight Fraction. *Euro-Asian Interstate Council for Standardization*. *Metrology and Certification* (2016). https://protect.gost.ru/document.aspx?control=7&id=202868
17. Copper Concentrates. Methods of Analysis. *Euro-Asian Interstate Council for Standardization*. *Metrology and Certification* (2014). https://internet-law.ru/gosts/gost/56292/
18. Copper and Complex Ores, and Products of Their Processing. Atomic Absorption Spectroscopy Method for Weight Fraction of Measurement of Copper, Zinc, Lead, Bismuth, Cadmium, Antimony. *Euro-Asian Interstate Council for Standardization.Metrology and Certification* (2016). https://protect.gost.ru/document.aspx?control=7&id=200313
19. Baerlocher Ch., McCusker L.B., Olson D.H. *Atlas of Zeolite Framework Types* (6th ed.). Amsterdam, Elsevier (2007). https://doi.org/10.1016/B978-0-444-53064-6.X5186-X
20. Tsitsishvili G.V., Andronikashvili T.G., et al. *Natural Zeolites*. UK, Chichester, Ellis Horwood (1991), 58. https://doi.org/10.1002/gj.3350290217
21. Aghamalyan N.R., Badalyan G.R., et al. Optical and EPR Spectroscopy of Natural Zeolite Modified by Microwave-Assisted Method. *J. Contemp. Physics* (*NAS RA*) **57** (2022), 370–376. https://doi.org/10.1134/S106833722204003X
22. Wang C., Cao L., Huang J. Influence of Acid Heat Treatment on the Structure and Water Vapor Adsorption Property of Natural Zeolite. *Surf. Interface Anal.* **49** (2017), 1249–1255. https://doi.org/10.1002/sia.6321
23. Rožić M., Cerjan-Stefanović Š., et al. Decationization and Dealumination of Clinoptilolite Tuff and Ammonium Exchange on Acid-modified Tuff. *J. Colloid Interface Sci*. **284** (2005), 48–56. https://doi.org/10.1016/j.jcis.2004.09.061
24. Tsitsishvili V.G., Dolaberidze N.M., et al. Acid and Thermal Treatment of Natural Heulandite. *Him. Fiz. Tehnol. Poverhni.* **14** (2023), 519–533. https://doi.org/10.15407/hftp14.04.519
25. Kukobat R., Škrbić R., et al. Thermal and Structural Stability of Microporous Natural Clinoptilolite Zeolite. *Microporous Mesoporous Mater*. **341**(2022). Article Number 112101.
26. Kukobat R., Škrbić R., et al. Thermal and Structural Stability of Microporous Natural Clinoptilolite Zeolite. *Microporous Mesoporous Mater*. **341**(2022). Article Number 112101. https://doi.org/10.1016/j.micromeso.2022.112101
27. Treacy M.M.J., Higgins J.B. *Collection of Simulated XRD Powder Patterns for Zeolites* (5th ed.). Amsterdam–London–New York–Oxford–Paris–Shannon–Tokyo, Elsevier (2007), 388. https://doi.org/10.1016/B978-0-444-53067-7.X5470-7

28. Tsitsishvili V., Dolaberidze N., et al. Properties of Georgian Heulandite-C linoptilolite and Its Application for Production of Bactericidal Adsorbents. *Scientific collection «InterConf»* **59** (2021), 633–642. https://ojs.ukrlogos.in.ua/index.php/interconf/article/view/13241
29. Szostak R. *Secondary Synthesis Methods, in Introduction to Zeolite Science and Practice* (eds. H. van Bekkum, E.M. Flanigen, P.A. Jacobs, J.C. Jansen). Elsevier (2001), 261–297. https://doi.org/10.1016/S0167-2991(01)80248-2
30. Mumpton F.A. Clinoptilolite Redefined. *Amer. Mineral.* **45** (1960), 351–369.
31. Tsitsishvili V., Panayotova M., et al. Acid Resistance and Ion-exchange Capacity of Natural Mixtures of Heulandite and Chabazite. *Minerals* **13** (2023), 364. https://doi.org/10.3390/min13030364
32. Olson D.H., Haag W.O., Borghard W.S. Use of Water as a Probe of Zeolitic Properties: Interaction of Water with HZSM-5. *Micropor. Mesopor. Mater*. **35-36** (2000), 435–446. https://doi.org/10.1016/S1387-1811(99)00240-1
33. Ates A., Hardacre C. The Effect of Various Treatment Conditions on Natural Zeolites: Ion Exchange, Acidic, Thermal and Stream Treatments. *J. Colloid Interf. Sci.* **372** (2012), 130–140. https://doi.org/10.1016/j.jcis.2012.01.017
34. Brunauer S., Deming L., et al. On a Theory of the van der Waals Adsorption of Gases. *J. Amer. Chem. Soc.* **62** (1940), 1723–1732. https://doi.org/10.1021/ja01864a025
35. Sing K.S.W., Everett D.H., et al. Reporting Physisorption Data for Gas/Solid Systems with Special Reference to the Determination of Surface Area and Porosity. *Pure Appl. Chem.* **57** (1985), 603–619. https://doi.org/10.1351/pac198557040603
36. Brunauer S., Emmett P.H., Teller E. Adsorption of Gases in Multimolecular Layers. *J. Amer. Chem. Soc.* **60** (1938), 309–319. https://doi.org/10.1021/ja01269a023
37. Barrett E.P., Joyner L.G., Halenda P.P. The Determination of Pore Volume and Area Distributions in Porous Substances. I. Computations from Nitrogen Isotherms. *J. Am. Chem. Soc*. **73** (1951), 373–380. https://doi.org/10.1021/ja01145a126
38. Halsey G.D. Physical Adsorption on Non-uniform Surfaces. *J. Chem. Phys.* **16** (1948), 931–937. https://doi.org/10.1063/1.1746689
39. Faass G.S. *Correlation of Gas Adsorption, Mercury Intrusion, and Electron Microscopy Pore Property Data for Porous Glasses.* US, Georgia Institute of Technology (1981). http://hdl.handle.net/1853/32965

Վ. Գ. ՑԻՑԻՇՎԻԼԻ, Ն. Ա. ՄԻՐՋՎԵԼԻ, Ն. Մ. ԴՈԼԱԲԵՐԻԴԶԵ, Մ. Օ. ՆԻՋԱՐԱԶԵ,
Չ. Ս. ԱՄԻՐԻՋԵ, Բ. Թ. ԽՈՒՑԻՇՎԻԼԻ, Լ. Շ. ԹԱՆԳԱՄՅԱՆ, Խ. Թ. ՆԱՋԱՐԵԹՅԱՆ,
Հ. Հ. ՍԱՐԳՍՅԱՆ, Ա. Վ. ՄԱՆՈՒԿՅԱՆ, Լ. Ռ. ՀԱՐՈՒԹՅՈՒՆՅԱՆ

ՆՈՐ ԿՈՂԲ ՀԱՆՔԱՎԱՅՐԻ ԿԼԻՆՈՊՏԻԼՈԼԻՏԻ ԹԹՎԱՅԻՆ ԵՎ ՋԵՐՄԱՅԻՆ ՄՇԱԿՈՒՄԸ

Բնական ցեոլիտի թթվային մշակումը հաճախ կիրառվում է ցեոլիտի ծակոտկեն կառուցվածքը և հատկությունները “բարելավելու” համար, որոնք փոփոխվում են նաև ջերմային մշակման արդյունքում: Քիմիական անալիզի, ռենտգենկառուցվածքային հետազոտության մեթոդներով, ջրի, բենզոլի և ազոտի ադսորբցիայի որոշմամբ ուսումնասիրվել է մինչև 2 *N* կոնցենտրացիայով աղաթթվի լուծույթների և մինչև 800°C ջերմային մշակման ազդեցությունը Հայաստանի Նոր Կողբ հանքավայրի կլինոպտիլոլիտ պարունակող

տուֆի կառուցվածքի և հատկությունների վրա, որն ընտրվել է նոր հակաբակտերիալ ֆիլտրող նյութեր ստեղծելու համար, որոնք պետք է կիրառվեն տարբեր ծագման ջրերի մաքրման և վարակազերծման համար: Հաստատված է, որ թթվային միջավայրը բերում է զգալի դեալյումինացման (Si/Al ատոմների հարաբերությունը մեծանում է ≈5-ից մինչև ≈9,4), իսկ կատիոնային բաղադրության փոփոխությունները առանց դեկատիոնիզացիայի բերում են ջրի գոլորշիները ադսորբելու ունակության նվազման. թթվային լուծույթները չեն նպաստում ցեոլիտի միկրոծակոտկեն բյուրեղային կառուցվածքի ամորֆիզացմանը, սակայն աստիճանաբար լուծում են այն: Թթվային մշակումը նաև "բացում" է միկրոծակոտիները ազոտի մեծ ոչ բևեռային մոլեկուլների համար, մեծացնում է ադսորբցիայի մակերևույթը և առաջացնում է փոփոխություններ մեզոծակոտկեն համակարգում, նպաստում դրանց չափսերի մեծացմանը: Ջերմային մշակումը 450°C-ում ձևափոխում է մասնակի դեհիդրատացված ցեոլիտը հեյլանդիտ B-ի մետաստաբիլ փազի, որին հաջորդում է ցեոլիտանման հանքանյութ վայրակիթի առաջացումը (500°C) և անորթիտանման դաշտային սպաթի առաջացումը (600°C); ամորֆ փազի պարունակությունը մեծանում է ջերմաստիճանի բարձրացմամբ, սակայն ցեոլիտի բնուրեղային կառուցվածքը պահպանվում է նույնիսկ 800°C-ում թրծելիս: Հեյլանդիտին բնորոշ ծակոտկենությունը (0,17 *սմ*^{3}/*գ*) պահպանվում է մինչև 700°C ջերմաստիճաններում մշակելիս, միկրոծակոտիների ադսորբցիայի տարողունակությունը ջրի գոլորշիների համար (>4 *մմոլ*/*գ*) չի փոփոխվում մինչև 500°C, ավելի բարձր ջերմաստիճաններում ազոտի մոլեկուլների համար մատչելի միկրոծակոտիների ծավալը և ադսորբցիայի մակերևույթը փոքրանում են, իսկ նանոչափի ծակոտիների միջին տրամագիծը մեծանում է:

В. Г. ЦИЦИШВИЛИ, Н. А. МИРДЗВЕЛИ, Н. М. ДОЛАБЕРИДЗЕ, М. О. НИДЖАРАДЗЕ,
З. С. АМИРИДЗЕ, Б. Т. ХУЦИШВИЛИ, Л. Ш. ТАНГАМЯН, Х. Т. НАЗАРЕТЯН,
А. О. САРГСЯН, А. В. МАНУКЯН, Л. Р. АРУТЮНЯН

КИСЛОТНАЯ И ТЕРМИЧЕСКАЯ ОБРАБОТКА АРМЯНСКОГО КЛИНОПТИЛОЛИТА

Кислотная обработка природного цеолита часто применяется для "улучшения" структуры и свойств, которые также подвержены влиянию термической обработки. Методами химического анализа, рентгеноструктурного анализа, адсорбции воды, бензола и азота изучено влияние растворов соляной кислоты до 2 *N* концентрации и температуры до 800°C на структуру и свойства туфа, содержащего клиноптилолит, из месторождения Нор Кохб (Армения), который выбран для создания новых бактерицидных цеолитовых фильтрующих материалов для очистки и дезинфекции вод из разных источников. Установлено, что кислотная среда приводит к значительному деалюминированию (соотношение атомов Si/Al растет ≈ от 5 до 9,4), а изменение катионного состава без декатионирования приводит к снижению адсорбционной емкости пара воды; кислотные растворы не приводят к аморфизации микропористой

кристаллической структуры, но постепенно растворяют ее. Также кислотная обработка “открывает” микропоры для больших неполярных молекул азота, увеличивает площадь адсорбции и приводит к изменениям системы мезопор, увеличивая их размеры. Термическая обработка при 457°C приводит к трансформации частично дегидратированного цеолита в метастабильную фазу гейландита B, с последующим возможным образованием цеолитоподобного минерала ваиракита (500°C) и анортит-подобного полевого шпата (600°C); содержание аморфной фазы увеличивается с ростом температуры, но кристаллическая структура цеолита остается без изменений даже после обжига при 800°C. Удельная пористость гейландита B (0,17 $см^3/г$) не меняется даже до 700°C, адсорбционная емкость микропор для пара воды (>4 *ммоль/г*) не меняется до 500°C, а при более высоких температурах объем микропор, доступных для молекул азота и площадь адсорбции уменьшаются, а средний диаметр наноразмерных пор увеличивается.